Characterization and reduction of artifacts in limited angle tomography

Jürgen Frikel[1,2], **Eric Todd Quinto**[3]

[1]Zentrum Mathematik, M6, Technische Universität München, Germany
[2]Institute of Computational Biology, Helmholtz Zentrum München, Germany
[3]Department of Mathematics, Tufts University, Medford, MA 02155, USA

E-mail: juergen.frikel@helmholtz-muenchen.de

E-mail: todd.quinto@tufts.edu

Abstract. We consider the reconstruction problem for limited angle tomography using filtered backprojection (FBP) and Lambda tomography. We use microlocal analysis to explain why the well-known streak artifacts are present at the end of the limited angular range. We explain how to mitigate the streaks and prove that our modified FBP and Lambda operators are standard pseudodifferential operators, and so they do not add artifacts. We provide reconstructions to illustrate our mathematical results.

Keywords: Computed Tomography, Lambda Tomography, Limited Angle Tomography, Radon transforms, Microlocal Analysis, Pseudodifferential operators.

Submitted to: *Inverse Problems*

1. Introduction

Computed tomography (CT) is one of the standard modalities in medical imaging. Its goal consists in finding the density $f : \mathbb{R}^2 \to \mathbb{R}$ of an unknown object by measuring and processing the attenuation of x-rays along a large number of lines through the object. The mathematical problem of this process consists in finding the density function f from the knowledge of its Radon transform

$$\mathcal{R}f(\theta, s) = \int_{-\infty}^{\infty} f(s\theta + t\theta^{\perp})\,\mathrm{d}t,$$

where $s \in \mathbb{R}$, $\theta \in S^1$, and $\theta^{\perp}$ is the unit vector $\pi/2$ radians counterclockwise from θ.

In the classical setting of CT the tomographic data $y = \mathcal{R}f(\theta, s)$ is assumed to be known for all values $(\theta, s) \in S^1 \times \mathbb{R}$. This tomographic problem has been extensively studied in the last decades and many reconstruction algorithms are available for complete data, see for example [27, 28]. Here, the most prominent reconstruction algorithm is the so-called Filtered Backprojection (FBP), which will be described in Section 2.2 of this article.

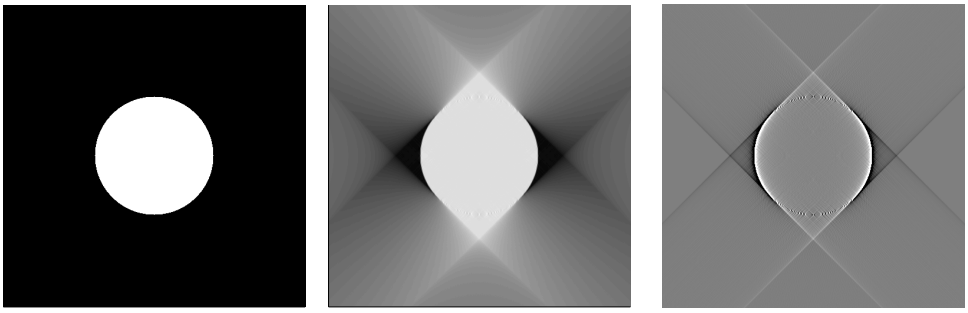

Figure 1 – Original image (left), Filtered Backprojection (FBP) reconstruction (middle) and Lambda reconstruction (right) for an angular range, $(-\Phi, \Phi)$ with $\Phi = 45^\circ$ (right). Note the streak artifacts and the missing boundaries in the limited angle reconstruction.

The success of CT has initiated the development of new tomographic imaging techniques where the tomographic data $\mathcal{R}f(\theta, s)$ is no longer available for all $(\theta, s) \in S^1 \times \mathbb{R}$, but is given only on a restricted subset of lines. Such data are called *limited tomographic data.*

Lambda tomography (Λ-CT) is an important algorithm related to FBP but that uses limited tomographic data. To image a function f at the point x using Λ-CT, one needs only data over lines that are arbitrarily close to x, so called Region of Interest (ROI) data. This algorithm does not reconstruct the object f but an image that emphasizes region boundaries and can provide high quality reconstructions. It is used for medical CT when doctors want to image only a small region in the body and it is used in micro-CT of industrial objects [6, 7, 45] (see also [21, 24, 39] for other local methods). We will describe this algorithm in Section 2.2.

The problem we study in this article is *limited angle tomography*: the data are restricted to lines in a limited angular range, i.e., $\mathcal{R}f(\theta, s)$ is known for all $s \in \mathbb{R}$ but for $\theta \in S^1_\Phi$ where S^1_Φ is a subset of S^1. Typical examples of modalities where such problems arise are digital breast tomosynthesis [29, 40], dental tomography [18, 26], or electron microscopy [3]. In electron microscopy limited angle Lambda CT is used for region of interest reconstruction [34]. In such situations, the problem is to reconstruct from data obtained using the limited angle Radon transform $\mathcal{R}_\Phi : f \mapsto \mathcal{R}f|_{S^1_\Phi \times \mathbb{R}}$, and the applications of existing reconstruction methods (originally designed for the full angular problem) are no longer straightforward. In fact, the problem is highly ill-posed, as can be seen from the singular values [23]. To this end, dedicated inversion methods were developed in [2, 14, 20, 22, 31, 37, 38, 44, 40]. However, in practice, the FBP algorithm is still the preferred reconstruction method, cf. for example [4, 5, 25, 30, 41, 42].

However, the FBP inversion formula requires completeness of the tomographic data. As a result, the use of the FBP algorithm in limited angle tomography reconstructs only specific features of the original object and creates additional artifacts in the reconstruction, cf. Figure 1. Though it is very well understood that only visible singularities can be reconstructed stably from a limited angle data [33], the artifacts at the ends of the angular range have not (to our knowledge) been heavily studied in the literature so far.

The main goals of this article are to explain why streak artifacts are generated by the FBP and Λ-CT algorithms for a limited angular range and to derive an artifact reduction strategy. Using the framework of microlocal analysis we will prove

characterizations of the artifacts in limited angle FBP and Λ-reconstructions. Those characterizations will precisely explain where and why artifacts are created by these algorithms. Based on these characterizations, we will explain how to mitigate those artifacts and construct versions of limited angle FBP and Λ-CT that do not produce added artifacts.

Microlocal analysis has been used to understand visible and invisible singularities as well as artifacts in other tomography problems besides X-ray CT, including cone beam CT [9], conical tilt electron microscopy [8], and an elegant abstract setting [13] that includes these cases. Added artifacts also occur in synthetic aperture Radar in the so-called left-right ambiguity [1, 43]. These problems are different from X-ray CT because the microlocal analysis is more subtle; for our transform and full data $\mathcal{R}^*\mathcal{R}$ is an elliptic pseudodifferential operator, and for these other problems, the reconstruction operators involving backprojection are not, in general, standard pseudodifferential operators, even for "complete" data. As a result, the artifact reduction strategies in [8, 9] only reduce the strength of artifacts; they do not eliminate them. In a more complicated setting in electron microscopy, the reduction strategy only reduces artifacts locally [35].

This paper is organized as follows. Section 2 of this article provides general definitions and basic facts about computed tomography and lambda CT. In particular, we define the reconstruction operators and characterize what these operators reconstruct for a limited angular range (Theorem 2.1). In Section 3, we review the framework of microlocal analysis including the notion of a singularity (wavefront set), and we recall the definition of a pseudodifferential operator. Our main results are presented in Section 4, where we use these concepts to derive precise characterizations of the microlocal properties of our reconstruction operators. Using this, we describe the added artifacts (Theorem 4.1). Moreover, we derive an artifact reduction strategy and prove that our modified reconstruction operators are standard pseudodifferential operators (Theorem 4.2). As a result, the modified reconstruction methods do not produce added artifacts (Corollary 4.3). Finally, in Section 5, we present some numerical experiments which illustrate our theory in practice. In the Appendix we prove a key theorem (Theorem A.1) and provide proofs of our main theorems.

2. Tomographic Reconstruction for a Limited Angular Range

In this section we define the FBP and Lambda reconstruction operators for the full angular range and investigate what these operators reconstruct when applied to limited angle data. We begin by fixing the notation and giving some basic definitions.

2.1. Notation and Basic Definitions

In what follows, $\mathcal{D}(\mathbb{R}^n)$ is the set of smooth functions on $\mathbb{R}^n$ with compact support, $\mathcal{S}(\mathbb{R}^n)$ is the Schwartz space of rapidly decreasing functions, and $\mathcal{E}(\mathbb{R}^n) = C^\infty(\mathbb{R}^n)$. Moreover, $\mathcal{D}'(\mathbb{R}^n)$ will denote the set of all distributions (i.e., the dual space to $\mathcal{D}(\mathbb{R}^n)$ with the weak-$*$ topology). The set of tempered distributions, $\mathcal{S}'(\mathbb{R}^n)$, is the dual space to $\mathcal{S}(\mathbb{R}^n)$, and the set of distributions with compact support is denoted by $\mathcal{E}'(\mathbb{R}^n)$, cf. [10, 17].

The Fourier transform of a function $f \in \mathcal{S}(\mathbb{R}^n)$ is defined as

$$\begin{aligned} \mathcal{F}f(\xi) = \hat{f}(\xi) &= (2\pi)^{-n/2} \int_{\mathbb{R}^n} e^{-ix\cdot\xi}\, f(x)\, \mathrm{d}x, \\ \mathcal{F}^{-1}f(x) = \check{f}(x) &= (2\pi)^{-n/2} \int_{\mathbb{R}^n} e^{ix\cdot\xi}\, f(\xi)\, \mathrm{d}\xi. \end{aligned} \tag{1}$$

The *Lambda operator* plays an important role in computed tomography. For $f \in \mathcal{S}(\mathbb{R}^n)$, we define

$$\Lambda_x f(\xi) = \mathcal{F}^{-1}\left(\|\xi\|\, \hat{f} \right), \tag{2}$$

and, as a pseudodifferential operator, $\Lambda_x = \sqrt{-\Delta}$ since $\|\xi\|^2$ is the symbol of $-\Delta$. Note that Λ_x is weakly continuous from $\mathcal{E}'(\mathbb{R}^2)$ to $\mathcal{S}'(\mathbb{R}^2)$ since it is a pseudodifferential operator [32].

We define the convolution on $\mathbb{R}^2$ using the factor $1/2\pi$:

$$f * g(x) = \frac{1}{2\pi} \int_{y\in\mathbb{R}^2} f(x-y) g(y) dy, \tag{3}$$

and with this definition, $\mathcal{F}(f * g) = (\mathcal{F}f)\,(\mathcal{F}g)$.

We further define $\mathcal{S}(S^1 \times \mathbb{R})$ and the partial Fourier transform for functions on $S^1 \times \mathbb{R}$. First, we say that the function $g(\theta, s) \in \mathcal{S}(S^1 \times \mathbb{R})$ if g is C^∞ on $S^1 \times \mathbb{R}$ and rapidly decreasing on $\mathbb{R}$ along with its derivatives, uniformly for $\theta \in S^1$. For $g \in \mathcal{S}(S^1 \times \mathbb{R})$ we define the partial Fourier transform and its inverse with respect to the second variable:

$$\begin{aligned} \mathcal{F}_s g(\theta, \tau) &= \frac{1}{\sqrt{2\pi}} \int_{\mathbb{R}} e^{-is\tau}\, g(\theta, s)\, \mathrm{d}s, \\ \mathcal{F}_s^{-1} g(\theta, s) &= \frac{1}{\sqrt{2\pi}} \int_{\mathbb{R}} e^{is\tau}\, g(\theta, \tau)\, \mathrm{d}\tau. \end{aligned} \tag{4}$$

Accordingly, we define the Lambda operator Λ_s for $g = g(\theta, s) \in \mathcal{S}(S^1 \times \mathbb{R})$ by

$$\Lambda_s g = \mathcal{F}_s^{-1}(|\tau| \mathcal{F}_s g\ ). \tag{5}$$

As noted above for Λ_x, the operator $\Lambda_s = \sqrt{-d^2/ds^2}$ is weakly continuous from $\mathcal{E}'(S^1 \times \mathbb{R})$ to $\mathcal{S}'(S^1 \times \mathbb{R})$.

2.2. Computed Tomography with Full Data

Here, we summarize the general definition and basic facts of CT and Λ-CT with data on a full angular range.

In what follows we let θ be a unit vector in S^1. When needed, we parametrize points on the unit sphere, S^1, using angles $\phi \in [-\pi, \pi]$:

$$\theta = \theta(\phi) = (\cos(\phi), \sin(\phi)), \qquad \theta^\perp = \theta^\perp(\phi) = (-\sin(\phi), \cos(\phi)) \tag{6}$$

where $\theta(\phi)$ is the unit vector in direction ϕ and $\theta^\perp(\phi) = \theta(\phi + \pi/2)$. For $(\theta, s) \in S^1 \times \mathbb{R}$, we define

$$L(\theta, s) = \left\{ x \in \mathbb{R}^2 : x \cdot \theta = s \right\}. \tag{7}$$

Note that $L(\theta, s)$ is the line which is perpendicular to θ and containing the point $s\theta$. Then the Radon transform of a function $f \in L^1(\mathbb{R}^2)$ is defined by

$$\mathcal{R}f(\theta, s) = \int_{L(\theta,s)} f(x)\,\mathrm{d}s = \int_{-\infty}^{\infty} f(s\theta + t\theta^{\perp})\,\mathrm{d}t, \tag{8}$$

where $\mathrm{d}s$ denotes the arc length measure on the line. The dual transform (or the backprojection operator) is defined for $g \in \mathcal{S}(S^1 \times \mathbb{R})$ as

$$\mathcal{R}^* g(x) = \int_{\theta \in S^1} g(\theta, x \cdot \theta)\,\mathrm{d}\theta, \tag{9}$$

which is the integral of g over all lines through x (since, for each θ, $x \in L(\theta, x \cdot \theta)$). One uses duality to show these transforms are both defined and weakly continuous for classes of distributions, and this is discussed at the start of the Appendix.

For $f \in \mathcal{S}(\mathbb{R}^2)$, a well-known inversion formula [27] for the Radon transform is

$$f = \frac{1}{4\pi}\mathcal{R}^*\left(\Lambda_s \mathcal{R}f\right) = \mathcal{B}(\mathcal{R}f), \tag{10}$$

where the reconstruction operator $\mathcal{B}$ is defined for $g \in \mathcal{S}(S^1 \times \mathbb{R})$ as

$$\mathcal{B}g = \frac{1}{4\pi}\mathcal{R}^*\left(\Lambda_s g\right). \tag{11}$$

The implementation of the inversion formula (10) is known as Filtered Backprojection (FBP) algorithm. Note that the reconstruction operator $\mathcal{B}$ may also be applied to distributions with compact support $g \in \mathcal{E}'(S^1 \times \mathbb{R})$ and the inversion formula (10) is valid for $f \in \mathcal{E}'(\mathbb{R}^2)$, cf. [27] and Theorem A.1.

Lambda tomography (Λ-CT) is a related reconstruction method [6, 7, 45]. For $g \in \mathcal{E}'(S^1 \times \mathbb{R})$

$$\mathcal{L}g = \frac{1}{4\pi}\mathcal{R}^*\left(-\frac{\partial^2}{\partial s^2} g\right), \tag{12}$$

and $\mathcal{L}$ does not reconstruct f but reconstructs $\Lambda_x f = \mathcal{L}\left(\mathcal{R}f\right)$ [7]. The advantage of Lambda CT is that it uses local data: To recover $\Lambda_x f(x)$, one needs only data $\mathcal{R}f$ over lines near x since $\left(-\frac{d^2}{ds^2}\right)$ is a local operator and $\mathcal{R}^*$ integrates over lines through x. A refinement proposed by Kennan Smith, which we will use, is to add a multiple of $\mathcal{R}^*\mathcal{R}f$ to provide contour to the reconstruction. Let $\mu \geq 0$ then

$$\mathcal{L}_\mu g = \frac{1}{4\pi}\mathcal{R}^*\left(-\frac{d^2}{ds^2} + \mu\right) g. \tag{13}$$

A straightforward calculation shows that

$$\mathcal{L}_\mu(\mathcal{R}f) = \Lambda_x f + f * \frac{\mu}{\|x\|} =: \Lambda_\mu f \tag{14}$$

where equation (14) gives the definition of $\Lambda_\mu f$ and we recall that the convolution is defined by (3). The term $\Lambda_x f$ highlights boundaries since it "takes a derivative", and the convolution term helps objects stand out from the background because the convolution with $\frac{\mu}{\|x\|}$ is more influenced by values of f near x (if f is large near x, so is the convolution). Note that $\mathcal{L} = \mathcal{L}_\mu$ for $\mu = 0$.

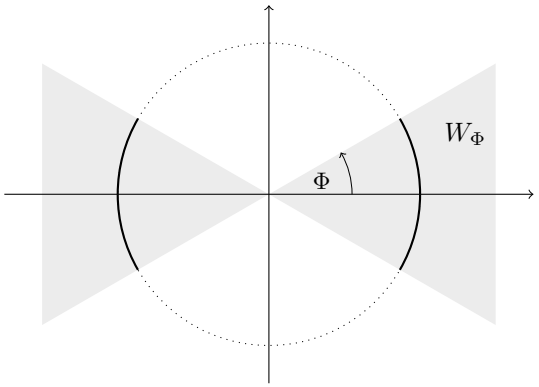

Figure 2 – The figure shows S^1_Φ (solid curve) as a subset of S^1 (dotted curve). The wedge $W_\Phi = \mathbb{R} \cdot S^1_\Phi$ is indicated by the gray shaded area.

2.3. Characterization of Limited Angle Reconstructions

In this work, we study the reconstruction problem for *limited angle tomography* where a portion of the projections $\mathcal{R}f$ is missing. That is, the data $\mathcal{R}f(\theta, s)$ is known only for $\theta \in S^1_\Phi \subsetneq S^1$ and $s \in \mathbb{R}$, where

$$S^1_\Phi := \left\{\theta \in S^1 : \theta = \pm(\cos\phi, \sin\phi), |\phi| < \Phi\right\} \tag{15}$$

and the *angular range parameter* Φ is assumed to satisfy $0 < \Phi < \pi/2$, cf. Figure 2. In order to compute a limited angle reconstruction, we therefore have to deal with the *limited angle Radon transform*

$$\mathcal{R}_\Phi : f \mapsto \mathcal{R}f\big|_{S^1_\Phi \times \mathbb{R}} \tag{16}$$

rather than data for all $\theta \in S^1$. We define the polar wedges

$$W_\Phi := \mathbb{R} \cdot S^1_\Phi = \left\{r\theta : \theta \in S^1_\Phi, r \in \mathbb{R}\right\}, \quad \text{and} \quad \overline{W}_\Phi = \mathrm{cl}(W_\Phi) \setminus \{0\}. \tag{17}$$

Moreover, we define the projection operator

$$P_\Phi f = \mathcal{F}^{-1}(\chi_{W_\Phi} \hat{f}), \tag{18}$$

where χ_{W_Φ} denotes the characteristic function of the set W_Φ.

The backprojection (or dual operator) for the limited angle Radon transform is given by

$$\mathcal{R}^*_\Phi g(x) = \int_{\theta \in S^1_\Phi} g(\theta, x \cdot \theta)\, \mathrm{d}\theta. \tag{19}$$

Since $\mathcal{R}^*_\Phi$ truncates the angles to S^1_Φ, evaluating $\mathcal{R}^*_\Phi$ on $\mathcal{R}f$ is the same as evaluating $\mathcal{R}^*_\Phi$ on $\mathcal{R}_\Phi f$. So, from now on, we will assume that we have data $\mathcal{R}f$, and we use $\mathcal{R}^*_\Phi$ to restrict the data. This will have the effect of reconstructing only using tomographic data for $(\theta, s) \in S^1_\Phi \times \mathbb{R}$, that is, reconstructing from limited angle data. This convention also makes the theory easier when we deal with distributions.

The operator $\mathcal{R}^*_\Phi$ is defined for $g \in \mathcal{S}(S^1 \times \mathbb{R})$ and it can be extended to g in the image $\mathcal{R}(\mathcal{E}'(\mathbb{R}^2))$ as noted in Theorem 2.1. With this observation in mind, for such g, we define

$$\mathcal{B}_\Phi g(x) = \frac{1}{4\pi} \mathcal{R}^*_\Phi \Lambda_s(g) \tag{20}$$

and the *limited angle filtered backprojection formula* is $\mathcal{B}_\Phi \mathcal{R} f$. We define the operators

$$\mathcal{L}_\Phi g = \frac{1}{4\pi} \mathcal{R}_\Phi^* \left(-\frac{d^2}{ds^2} g \right), \tag{21}$$

and, for $\mu \geq 0$,

$$\mathcal{L}_{\mu,\Phi} g = \frac{1}{4\pi} \mathcal{R}_\Phi^* \left(-\frac{d^2}{ds^2} + \mu \right) g. \tag{22}$$

These give two *limited angle Lambda reconstruction formulas* $\mathcal{L}_\Phi \mathcal{R} f$ and $\mathcal{L}_{\mu,\Phi} \mathcal{R} f$. Since the limited angle data $g = \mathcal{R}_\Phi f$ is highly incomplete, we cannot expect to obtain the function f by applying the filtered backprojection reconstruction formula (20) to data g. Similarly, we cannot expect to recover $\Lambda_x f$ by applying $\mathcal{L}_\Phi$. However, we can precisely characterize what these operators do reconstruct.

Theorem 2.1. *Let $f \in \mathcal{S}(\mathbb{R}^2)$. Then, the limited angle FBP reconstruction formula* (20) *satisfies*

$$\mathcal{B}_\Phi(\mathcal{R} f) = P_\Phi f \tag{23}$$

and the limited angle Lambda CT formulas

$$\mathcal{L}_\Phi(\mathcal{R} f) = P_\Phi(\Lambda_x f), \qquad \mathcal{L}_{\mu,\Phi}(\mathcal{R} f) = P_\Phi(\Lambda_\mu f). \tag{24}$$

These formulas are also valid for $f \in \mathcal{E}'(\mathbb{R}^2)$ in the sense that $\mathcal{R} f$ is a distribution on $S^1 \times \mathbb{R}$ on which Λ_s and $-d^2/ds^2$ can be applied and $\mathcal{R}_\Phi^*$ can be applied on the image of such distributions. Furthermore, the maps, $\mathcal{B}_\Phi \mathcal{R}$, $\mathcal{L}_\Phi \mathcal{R}$ and $\mathcal{L}_{\mu,\Phi} \mathcal{R}$ are all weakly continuous from $\mathcal{E}'(\mathbb{R}^2)$ to $\mathcal{S}'(\mathbb{R}^2)$.

Thus, these limited angle formulas recover P_Φ of what the full-angle formulas recover. The proof will be given in the appendix since it follows from a more general theorem proven there. A calculation similar to equation (23) was proven by Tuy [44].

3. Microlocal Analysis and Pseudodifferential Operators

The concepts in this section will allow us to characterize the streaks in Figure 1. Microlocal analysis is a powerful concept which enables us to describe simultaneously the locations $x \in \mathbb{R}^n$ and directions $\xi \in \mathbb{R}^n_*$ of singularities of a distributions. For general facts about the theory of distributions and more details on microlocal analysis we refer to [10, 17].

Here and in what follows we will use the notation

$$\mathbb{R}^n_* = \mathbb{R}^n \setminus \{0\}.$$

A function $f(\xi)$ is said to *decay rapidly in* a conic open set V if it decays faster than any power of $1/\|\xi\|$ in V. The singular support of a distribution, f, $\operatorname{sing\,supp}(f)$, is the complement of the largest open set on which f is a C^∞ function. It follows directly from this definition that $\operatorname{sing\,supp}(f) \subset \operatorname{supp}(f)$, and $\operatorname{sing\,supp}(f) = \emptyset$ if and only if $f \in C^\infty(\mathbb{R}^n)$.

Definition 3.1 (Frequency Set [17, §8.1])**.** Let $f \in \mathcal{E}'(\mathbb{R}^n)$. We define the *frequency set* $\Sigma(f)$ *of* f as the set of all directions $\xi \in \mathbb{R}^n_*$ in which $\hat{f}$ does not decay rapidly in any conic neighborhood of ξ.

We note the following fundamental property [17, Lemma 8.1.1] of the frequency set: For $f \in \mathcal{E}'(\mathbb{R}^n)$ and $\varphi \in \mathcal{D}(\mathbb{R}^n)$ it holds

$$\Sigma(\varphi f) \subset \Sigma(f). \tag{25}$$

The singular support $\operatorname{sing\,supp}(f)$ of a distribution gives the location of the singularities, whereas, the frequency of set $\Sigma(f)$ describes, in some sense, all directions in which f is singular. However, both concepts are not yet correlated; if $\Sigma(f) \neq \emptyset$, then $f \notin C^\infty(\mathbb{R}^n)$, but we don't know the location of the singularity(ies) corresponding to any $\xi \in \Sigma(f)$. The notion of a wavefront set combines both of these concepts and simultaneously describes the location and the direction of a singularity. In order to define the wavefront set, we first need the following notion of a localized frequency set.

Definition 3.2 (Localized Frequency Set)**.** Let $f \in \mathcal{D}'(\mathbb{R}^n)$. The *localized frequency set* of f at $x \in \mathbb{R}^n$ is defined as

$$\Sigma_x(f) = \bigcap \{\Sigma(\varphi f) : \varphi \in \mathcal{D}(\mathbb{R}^n), \varphi(x) \neq 0\}. \tag{26}$$

We first note that, by (25), $\Sigma_x(f) \subset \Sigma(f)$. Therefore, the localized frequency set $\Sigma_x(f)$ of f at x can be interpreted as the set of directions in which f is singular at x. This gives us a definition of singularity that includes location and direction.

Definition 3.3 (Wavefront Set)**.** Let $f \in \mathcal{D}'(\mathbb{R}^n)$. The *wavefront set* of f is given by

$$\mathrm{WF}(f) = \{(x, \xi) \in \mathbb{R}^n \times \mathbb{R}^n_* : \xi \in \Sigma_x(f)\}. \tag{27}$$

If $(x, \xi) \notin \mathrm{WF}(f)$ one says that f is *microlocally smooth near* (x, ξ).

The frequency set $\Sigma(f)$ is the projection of $\mathrm{WF}(f)$ on the second coordinate ([17, Proposition 8.1.3]) and $\operatorname{sing\,supp}(f)$ is the projection onto the first coordinate.

Now we specialize to $\mathbb{R}^2$ in preparation for our tomography problem.

Example 3.1. Let $\Omega \subset \mathbb{R}^2$ be such that the boundary $\partial\Omega$ is a smooth manifold. Then, the wavefront set of χ_Ω is the set of normal vectors to the boundary of Ω:

$$(x, \xi) \in WF(\chi_\Omega) \quad \Leftrightarrow \quad x \in \partial\Omega,\ \xi \in N_x, \tag{28}$$

where χ_Ω denotes the characteristic function of Ω and N_x is the normal space to $\partial\Omega$ at $x \in \partial\Omega$. The proof of this fact is non-trivial and we refer the reader to [17, p. 265].

For $\Phi \in (0, \pi/2)$ and $f \in \mathcal{D}'(\mathbb{R}^2)$, we define

$$\mathrm{WF}_\Phi(f) = \mathrm{WF}(f) \cap \left(\mathbb{R}^2 \times W_\Phi\right) \tag{29}$$

and

$$\mathrm{WF}_{\overline{\Phi}}(f) = \mathrm{WF}(f) \cap \left(\mathbb{R}^2 \times \overline{W}_\Phi\right). \tag{30}$$

These sets represent the part of $\mathrm{WF}(f)$ that is in W_Φ or $\overline{W}_\Phi$ and they will be important when we analyze the limited angle operators in the next section.

In this article we will use some facts from the theory of pseudodifferential operators (PSIDOs), which we now define. For functions $f \in \mathcal{D}(\mathbb{R}^n)$, the operator

$$\mathcal{P}f(x) = \frac{1}{(2\pi)^n} \int_{\xi \in \mathbb{R}^n} e^{ix\cdot\xi}\, a(x, \xi) \mathcal{F}f(\xi)\, \mathrm{d}\xi \tag{31}$$

is a PSIDO of order $m \in \mathbb{R}$ if its symbol $a(x,\xi)$ satisfies the following bounds at ∞ in ξ: for each compact set $K \subset \mathbb{R}^n$, and any two multi-indices α and β in $\{0,1,2,\dots\}^n$ there is a constant $C_{K,\alpha,\beta}$ such that

$$\forall x \in K \; \forall \xi \in \mathbb{R}^n, \|\xi\| > 1, \; \left| D_x^\alpha D_\xi^\beta a(x,\xi) \right| \leq C_{K,\alpha,\beta}(1+\|\xi\|)^{m-|\beta|},$$

where $|\beta|$ is the order of the differential operator D^β. Because of our application, we assume $a(x,\xi)$ is locally integrable and smooth away from $\xi = 0$; in the usual definition, a is assumed to be C^∞ everywhere. Any operator with such a singularity at $\xi = 0$ can be written as pseudodifferential operator with C^∞ symbol plus a smoothing operator, so its properties are the same as in the case for operators with smooth symbols at $\xi = 0$. In what follows, we need only to consider a very classical type of PSIDO on $\mathcal{E}'(\mathbb{R}^2)$: operators whose symbol $a(x,\xi)$ is a sum of a finite number of terms each of which is homogeneous in ξ and smooth away from the origin. Such operators satisfy the bounds to be PSIDOs [32, p. 198, §6]. For example, the operator Λ_μ is a PSIDO of order one with symbol $a(x,\xi) = \|\xi\| + \frac{\mu}{\|\xi\|}$ as can be seen from (14). We refer to [32] for the properties of pseudodifferential operators.

Pseudodifferential operators satisfy the *pseudolocal property*, namely if $\mathcal{P}$ is a PSIDO and $f \in \mathcal{E}'(\mathbb{R}^2)$, then $\mathrm{WF}(\mathcal{P}f) \subset \mathrm{WF}(f)$. This means that any PSIDO $\mathcal{P}$ does not add singularities to the "reconstruction" $\mathcal{P}f$ that are not already present in f.

A PSIDO $\mathcal{P}$ with symbol $a(x,\xi)$ is *elliptic of order* $m \in \mathbb{R}$ *on an open conic set* $V \subset \mathbb{R}^n$ if the operator is order m and for each compact set $K \subset \mathbb{R}^n$, there are constants $c_K > 0$ and L_K such that for all $x \in K$ and $\xi \in V$ with $\|\xi\| > L_K$, $c_K\,(1+\|\xi\|)^m \leq |a(x,\xi)|$. If $\mathcal{P}$ is elliptic in V then singularities of f in directions in V will show up in $\mathcal{P}f$, that is if $\xi \in V$ and $(x,\xi) \in \mathrm{WF}(f)$, then $(x,\xi) \in \mathrm{WF}(\mathcal{P}f)$.

4. Characterization and Reduction of Limited Angle Artifacts

This section contains our main results. Here, we will explain why and where added singularities are generated and prove an artifact reduction strategy. In the first part we will present a precise characterization of microlocal properties of the operators (20)-(22). In the second part, we will define modified reconstruction operators and prove that they are standard pseudodifferential operators and thus do not produce streak artifacts.

4.1. Characterization of Limited Angle Artifacts

We begin by deriving a precise characterization of the microlocal properties of our reconstruction operators, including the added artifacts at the ends of the angular range.

Theorem 4.1 (Characterization of Limited Angle Artifacts)**.** *Let* $\Phi \in [0, \pi/2)$ *and let* $f \in \mathcal{E}'(\mathbb{R}^2)$*. Let* $\mathcal{H}$ *be any one of the operators* $\mathcal{B}_\Phi$, $\mathcal{L}_\Phi$, $\mathcal{L}_{\mu,\Phi}$ *defined in* (20)-(22)*. Then*

$$\mathrm{WF}_\Phi(f) \subset \mathrm{WF}\left(\mathcal{H}(\mathcal{R}f)\right) \subset \mathrm{WF}_{\overline{\Phi}}(f) \cup \mathcal{A}_\Phi(f), \tag{32}$$

where

$$\mathcal{A}_\Phi(f) = \left\{ (x + r\theta^\perp(\phi), \alpha\theta(\phi)) : (x, \alpha\theta(\phi) \in \mathrm{WF}(f),\, r, \alpha \in \mathbb{R}_*,\, \phi = \pm\Phi \right\} \tag{33}$$

is the set of possible added singularities in the reconstruction $\mathcal{H}\mathcal{R}f$*.*

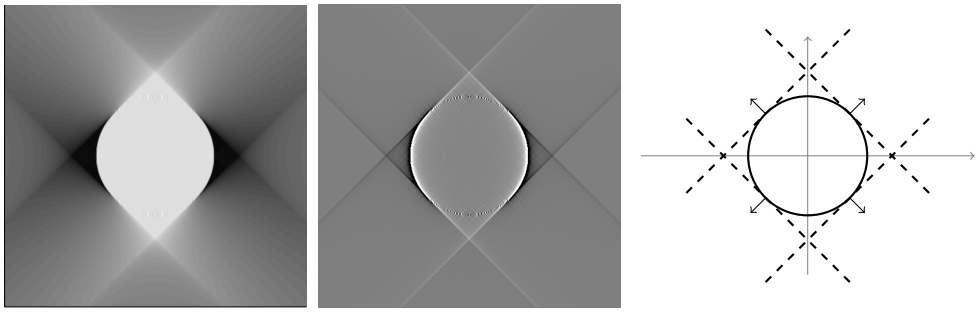

Figure 3 – Filtered backprojection reconstruction of $\chi_{B(0,1)}$ (left) and Lambda reconstruction of $\chi_{B(0,1)}$ (middle), both windowed display, at an angular range $[-\Phi, \Phi]$, $\Phi = 45^\circ$ and an illustration of added singularities (right). According to Theorem 4.1, the additional singularities (streak artifacts) are located on lines $l(r) = x_f + r\theta(\pm\Phi)$, where x_f is such that $(x_f, \alpha\theta(\pm\Phi)) \in \mathrm{WF}(f)$, $\alpha \neq 0$. The correspondence of the theoretical description (right) and practical reconstructions (left + middle) is remarkable, cf. Theorem 4.1.

The theorem is proved in the appendix because the proof is technical and it relies heavily on the key theorem of that section, Theorem A.1.

Theorem 4.1 is of particular interest for limited angle tomography since it provides a precise characterization of the wavefront set of limited angle filtered backprojection and Lambda reconstructions. In particular, it explains all effects that we observed in reconstructions that we showed in the introduction of this article (cf. Figure 1). For this discussion, let $\mathcal{H}$ be any of the operators $\mathcal{B}_\Phi$, $\mathcal{L}_\Phi$, or $\mathcal{L}_{\mu,\Phi}$. First, note that the only singularities of f that are visible from our reconstruction operators are those with directions in $\overline{W}_\Phi$; singularities of f with directions outside $\overline{W}_\Phi$ will be smoothed by $\mathcal{HR}$. This is true because of containment (32); since the right-hand term includes only such singularities so the left hand term does, too. This is to be expected because a singularity of f at (x, ξ) is visible from Radon data $\mathcal{R}f$ in a neighborhood of (θ, s) if and only if the line $L(\theta, s)$ contains x and is normal to ξ (e.g., [33]). So, if a singularity is not normal to a line in the data set, it will not be imaged.

With this in mind, we will call a singularity of f at (x, ξ) *visible* from limited angle data (with $\theta \in S^1_\Phi$) if $\xi \in W_\Phi$. We justify this by noting that $\mathrm{WF}_\Phi(f) \subset \mathrm{WF}(\mathcal{HR}f)$ by (32). We exclude singularities at $\theta(\pm\Phi)$ from this definition because they could also be added singularities as we now explain.

Each singularity in $\mathcal{A}(f)$ will be called *an added singularity* since it comes from a singularity of f at a different point. If $(x, \xi) \in \mathrm{WF}(f)$ in one of the four directions $\pm\theta(\pm\Phi)$, then the added singularities are on the line through x normal to ξ. That is, if ξ is parallel to $\theta(\pm\Phi)$, and $(x, \xi) \in \mathrm{WF}(f)$, then singularities of the limited angle operators (20)-(22) can occur at any point along the line through x and perpendicular to ξ. This is seen in the reconstructions in Figure 1; the artifacts are created along lines at the end of the data set that are perpendicular to singularities of f as these lines correspond to $\phi = \pm\Phi$. An illustration of this discussion is shown in Figure 3.

We conclude this section by noting that a good reconstruction algorithm, on the one hand, should be able to reliably reconstruct visible singularities, and on the other hand, avoid the production of the added singularities.

4.2. Reduction of Limited Angle Artifacts

Our aim in this section is to derive an artifact reduction strategy for the limited angle filtered backprojection (FBP) algorithm, $\mathcal{B}_\Phi$, and the limited angle Lambda operators $\mathcal{L}_\Phi$ and $\mathcal{L}_{\mu,\Phi}$. In order to reduce artifacts, our idea consists in modifying the above reconstruction formulas in such a way that they output a function $T_\Phi f$ which

(i) does not include additional singularities, i.e., $\mathrm{WF}(T_\Phi f) \subset \mathrm{WF}_\Phi(f)$,

(ii) is a good approximation to $P_\Phi f$ (or for limited angle Lambda CT a good approximation to $P_\Phi \Lambda_\mu$).

(iii) contains most of the visible singularities of f, i.e., for some $\Phi' \in (0, \Phi)$, $\mathrm{WF}_{\Phi'}(f) \subset \mathrm{WF}(T_\Phi f)$ (where $\mathrm{WF}_{\Phi'}(f)$ is the part of the wavefront set of f with directions in $W_{\Phi'}$).

Let us first point out why $P_\Phi f = \mathcal{F}^{-1}(\chi_{W_\Phi} \hat{f})$ may contain singularities (x, ξ) which do not belong to the wavefront set of f. To this end, we write

$$\mathcal{B}_\Phi \mathcal{R} f = \frac{1}{4\pi} f * \check{u}_\Phi,$$

where $\check{u}_\Phi = \mathcal{F}^{-1}(\chi_{W_\Phi})$. Then, by examining the proof of Theorem 4.1 (in particular the part between (A.17) and (A.20)) it is easy to see that the set of additional singularities $\mathcal{A}_\Phi(f)$ may be written as

$$\mathcal{A}_\Phi(f) = \left\{(x+y, \xi) \in \mathbb{R}^2 \times \mathbb{R}^2_* : (x, \xi) \in \mathrm{WF}(f),\, (y, \xi) \in \mathrm{WF}(\check{u}_\Phi),\, y \neq 0\right\}.$$

Therefore, by the "duality" for wavefront set of homogeneous distributions and their Fourier transforms, Lemma A.4, added singularities are produced because $\operatorname{sing\,supp}(u_\Phi) \neq \{0\}$. To clarify this point, if $\operatorname{sing\,supp}(u_\Phi)$ *were* $\{0\}$, then the only singularities in the convolution $f * \check{u}_\Phi$ would be those from f. However, since $\operatorname{sing\,supp}(u_\Phi)$ is larger, artifacts can be added to the convolution and hence to $\mathcal{B}_\Phi \mathcal{R} f$. In order to avoid the production of added singularities, it is therefore appropriate to aim at replacing u_Φ by a homogeneous distribution with a smooth Fourier transform on $\mathbb{R}^2_*$ (i.e., away from the origin).

Another way to say this is to note that $\mathcal{B}_\Phi \mathcal{R}$ is not a standard pseudodifferential operator because its symbol is not smooth. This is seen from (A.2b) with $\mathcal{K} = \chi_{S^1_\Phi}$: the symbol of $\mathcal{B}_\Phi \mathcal{R}$, $\chi_{S^1_\Phi}(\xi)$, is not smooth.

Remark 1. To come up with an artifact reduction strategy, we will consider more general weights for the backprojection. We define the multiplication operator

$$\begin{gathered} \mathcal{K} : \mathcal{S}(S^1 \times \mathbb{R}) \to \mathcal{S}'(S^1 \times \mathbb{R}),\ \mathcal{K} g(\theta, s) = \kappa(\theta) g(\theta, s) \\ \text{where}\ \ \kappa : S^1 \to \mathbb{R}, \qquad \operatorname{supp}(\kappa) \subset \mathrm{cl}(S^1_\Phi) \end{gathered} \tag{34}$$

and use $\mathcal{K}$ as a cutoff for the weighted backprojection: $\mathcal{R}^* \mathcal{K}$.

If $\kappa = \chi_\Phi$, then $\mathcal{R}^* \mathcal{K} = \mathcal{R}^*_\Phi$. In general, since $\operatorname{supp}(\kappa) \subset \mathrm{cl}(S^1_\Phi)$, then $\mathcal{R}^* \mathcal{K}$ uses only limited angle data for $\theta \in \mathrm{cl}(S^1_\Phi)$, so $\mathcal{R}^* \mathcal{K}$ is a weighted limited angle backprojection.

Furthermore, if κ is in $C^\infty(S^1)$, then as we will claim in Corollary 4.3, $\mathcal{B}_\Phi \mathcal{K}$ and $\mathcal{L}_{\mu,\Phi} \mathcal{K}$ will not add singularities to the reconstructions, as suggested just above this remark.

Although one cannot, in general, evaluate $\mathcal{R}^*\mathcal{K}$ on arbitrary distributions in $\mathcal{S}'(S^1 \times \mathbb{R})$, we will prove (Theorem A.1) that one can evaluate $\mathcal{R}^*\mathcal{K}$ on distributions in $\mathcal{R}(\mathcal{E}'(\mathbb{R}^2))$ as long as κ is piecewise continuous. Separating out the weight $\mathcal{K}$ from the backprojection makes the discussion more general and useful, and we will take this viewpoint from now on.

Theorem 4.2. *Let $\kappa : S^1 \to \mathbb{R}$ be a smooth function and assume* $\operatorname{supp}(\kappa) \subset \operatorname{cl}(S^1_\Phi)$. *Let $\mathcal{K}$ be the operator that multiplies by κ*

$$\mathcal{K}g(\theta, s) = \kappa(\theta)g(\theta, s)\,.$$

Then the operators

$$\mathcal{B}_\Phi\mathcal{K}\mathcal{R}, \quad \mathcal{L}_\Phi\mathcal{K}\mathcal{R}, \quad \mathcal{L}_{\mu,\Phi}\mathcal{K}\mathcal{R} \tag{35}$$

are all standard pseudodifferential operators and their full symbols are, respectively,

$$\kappa\left(\frac{\xi}{\|\xi\|}\right), \quad \kappa\left(\frac{\xi}{\|\xi\|}\right)\|\xi\|\,, \quad \kappa\left(\frac{\xi}{\|\xi\|}\right)\left(\|\xi\| + \frac{\mu}{\|\xi\|}\right). \tag{36}$$

Our next corollary shows that using a smooth cutoff, κ, on S^1_Φ does achieve the goals listed in items (i)-(iii).

Corollary 4.3 (Reduction of Limited Angle Artifacts)**.** *Let $\kappa : S^1 \to \mathbb{R}$ be a smooth function supported in* $\operatorname{cl}(S^1_\Phi)$ *and assume $\Phi' \in (0, \Phi)$ and $\kappa = 1$ on $S_{\Phi'}$. Assume $\mathcal{H}$ is any one of the operators $\mathcal{B}_\Phi\mathcal{K}$, $\mathcal{L}_\Phi\mathcal{K}$, $\mathcal{L}_{\mu,\Phi}\mathcal{K}$ for this κ and $f \in \mathcal{E}'(\mathbb{R}^2)$. Then*

$$\mathrm{WF}_{\Phi'}(f) \subset \mathrm{WF}(\mathcal{H}\mathcal{R}f) \subset \mathrm{WF}_\Phi(f) \tag{37}$$

and each of the operators

$$(\mathcal{B}_\Phi\mathcal{K}\mathcal{R} - \mathcal{B}_\Phi\mathcal{R})\,, \quad (\mathcal{L}_\Phi\mathcal{K}\mathcal{R} - \mathcal{L}_\Phi\mathcal{R})\,, \quad (\mathcal{L}_{\mu,\Phi}\mathcal{K}\mathcal{R} - \mathcal{L}_{\mu,\Phi}\mathcal{R}) \tag{38}$$

is a smoothing operator for directions in $W_{\Phi'}$ (i.e., for $(\mathcal{B}_\Phi\mathcal{K}\mathcal{R} - \mathcal{B}_\Phi\mathcal{R})$, if $f \in \mathcal{E}'(\mathbb{R}^2)$, then $\mathrm{WF}((\mathcal{B}_\Phi\mathcal{K}\mathcal{R} - \mathcal{B}_\Phi\mathcal{R})\,f) \cap \mathbb{R}^2 \times W_{\Phi'} = \emptyset$*).*

Theorem 4.2 and Corollary 4.3 will be proven in the appendix since they depend on the key theorem of that section, Theorem A.1.

Corollary 4.3 shows that using a smooth κ achieves the goals at the start of this section; (37) shows that goal (i) and (ii) at the start of this section hold. Then, since each of the operators in (38) (e.g., $\mathcal{B}_\Phi\mathcal{K}\mathcal{R} - \mathcal{B}_\Phi\mathcal{R}$), is smoothing for directions in $W_{\Phi'}$, the smoothed operator (e.g., $\mathcal{B}_\Phi\mathcal{K}\mathcal{R}$) has the singularities at the same points and of the same order as the non-smoothed one (e.g., $\mathcal{B}_\Phi\mathcal{R}$), at least for directions in $W_{\Phi'}$. This shows goal (iii) is satisfied. So, a preprocessing of the data $\mathcal{R}f$, namely the multiplication of the data by the smooth function κ in (34) and the subsequent application of $\mathcal{B}_\Phi$, $\mathcal{L}_\Phi$ or $\mathcal{L}_{\mu,\Phi}$ leads to reconstructions that do not contain added artifacts. Furthermore, we now understand why these artifacts appear without preprocessing.

5. Reconstructions

The goal of this section it is to verify the results of Section 4.2 numerically. In order to implement our artifact reduction strategy, we need a smooth (i.e. $C^\infty(S^1)$) cutoff

function $\kappa_\varepsilon : S^1 \to \mathbb{R}$ which satisfies the assumptions of Corollary 4.3. Then, the multiplication operator

$$\mathcal{K}_\varepsilon g(\theta, s) = \kappa_\varepsilon(\theta) g(\theta, s)$$

will satisfy the assumptions of Theorem 4.2 and therefore may be used for artifact reduction.

In what follows, we let $0 < \varepsilon < \pi/2$ and define $\varphi_\varepsilon : [-\pi, \pi] \to [0, 1]$ to be a π-periodic function which is given by $\varphi_\varepsilon(x) = \exp(\frac{x^2}{x^2-\varepsilon^2})$ for $|x| \leq \varepsilon$ and $\varphi_\varepsilon(x) = 0$ for $\varepsilon < |x| < \pi/2$. Then, we define the cutoff function $\kappa_\varepsilon : S^1 \to \mathbb{R}$ via

$$\kappa_\varepsilon(\theta(\phi)) = \begin{cases} \varphi_\varepsilon(\phi + (\Phi - \varepsilon)), & \phi \in [-\Phi, -(\Phi - \varepsilon)], \\ 1, & \phi \in [-(\Phi - \varepsilon), \Phi - \varepsilon], \\ \varphi_\varepsilon(\phi - (\Phi - \varepsilon)), & \phi \in [(\Phi - \varepsilon), \Phi], \\ 0, & \text{else}, \end{cases} \tag{39}$$

where $\phi \in [-\pi, \pi)$. Note that $\kappa_\varepsilon \equiv 1$ on $S^1_{\Phi-\varepsilon}$ and has smooth transition from 1 to 0 in $S^1_\Phi \setminus S^1_{\Phi-\varepsilon}$. Although the κ_ε is not smooth at $\pm\theta(\pm\Phi)$, we may use it for artifact reduction because, in practice, it is evaluated at a finite number of points and there is a smooth function that has these values at these points.

We have implemented our modified reconstruction operators $\mathcal{B}_\Phi\mathcal{K}_\varepsilon$, $\mathcal{L}_\Phi\mathcal{K}_\varepsilon$ and $\mathcal{L}_{\mu,\Phi}\mathcal{K}_\varepsilon$ for parallel geometry in Matlab using the function κ_ε which is defined in (39). The resulting reconstructions for $\varepsilon \in \{0°, 20°, 40°\}$ are shown in Figure 4 and Figure 5. Here, one can clearly observe the effect of artifact reduction: While the limited angle artifacts are visible in FBP and Lambda reconstructions (left column), the implementation of the artifact reduction strategy, using a cutoff κ_ε in the operator $\mathcal{K}_\varepsilon$, mitigates the production of the added singularities (middle and right column).

Remark 2. Note that the cutoff function κ_ε satisfies $\kappa_\varepsilon(\pm\theta(\pm\Phi)) = 0$. According to that, the data which is given by projections with respect to orientations $\pm\theta(\pm\Phi)$ is not used by the algorithm. To account for that, we set $\kappa_\varepsilon(\pm\theta(\pm\Phi)) = \delta$, for some small $\delta > 0$, in the practical implementation of our artifact reduction strategy.

Next, let us comment on the choice of the parameter $\varepsilon \in (0, \Phi]$ in (39). For convenience, let's talk just about $\mathcal{B}_\Phi$. The analogous statements hold for $\mathcal{L}_\Phi$ and $\mathcal{L}_{\mu,\Phi}$. Firstly, according to Theorem 4.2 every choice of the parameter $\varepsilon \in (0, \Phi]$ leads to a reconstruction which does not contain additional artifacts as opposed to $\mathcal{B}_\Phi\mathcal{R}$. Secondly, the function κ_ε converges pointwise to χ_{W_Φ} as $\varepsilon \to 0$. Therefore, a small value of the parameter ε ensures that $\mathcal{B}_\Phi\mathcal{K}_\varepsilon\mathcal{R}f$ is close to $\mathcal{B}_\Phi\mathcal{R}f = P_\Phi f$ (cf. requirement (ii) and that $\mathcal{B}_\Phi\mathcal{K}_\varepsilon\mathcal{R}f - \mathcal{B}_\Phi\mathcal{R}_\Phi f$ is smoothing in $\mathbb{R}^2 \times W_{\Phi'}$). That is, a small parameter ε leads to a reconstruction which is a good approximation to $\mathcal{B}_\Phi\mathcal{R}f$ and does not contain additional artifacts, i.e., the requirements (i)-(iii) are satisfied. Moreover, note that by (38), $\mathcal{B}_\Phi\mathcal{K}_\varepsilon\mathcal{R}f$ has singularities at the same locations in $\mathbb{R}^2 \times W_{\Phi'}$ as f does (and as $\mathcal{B}_\Phi\mathcal{R}f$ does). However, for small values of ε the streaks might still be visible in the reconstructions, at least near $\mathrm{supp}(f)$, as can be seen from the middle column of Figure 4. This is because κ_ε decays very rapidly near the boundary ∂W_Φ for small values of ε so singularities are smoothed, but their derivatives can still be large. On the other hand, large values of ε may lead to smoothing of visible singularities with directions near $\pm\theta(\pm\Phi)$. This effect can be particularly observed in Figure 5 by comparing left and right columns, where the original image has many singularities with directions near $\pm 45°$. To sum up, we observe a trade-off between

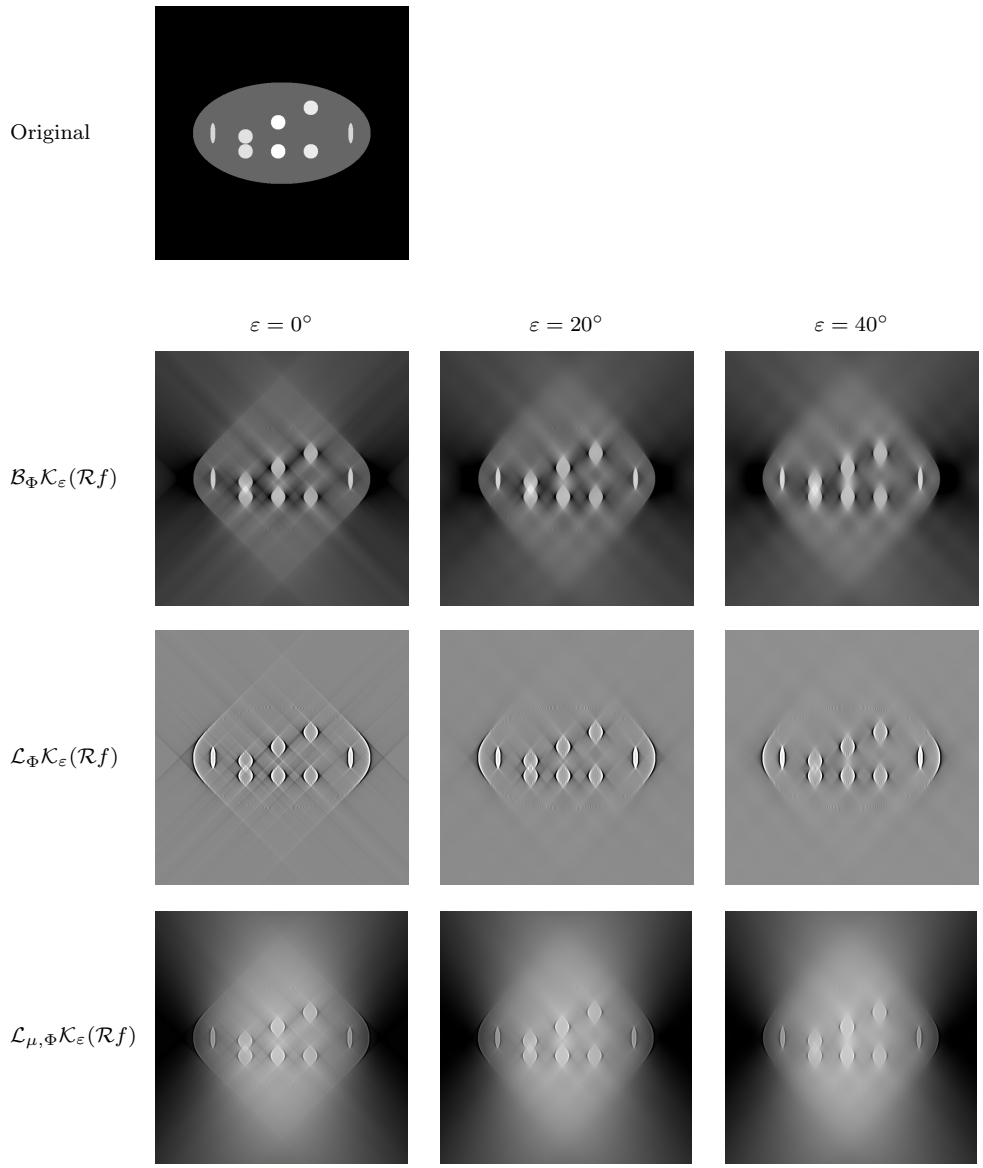

Figure 4 – Reconstruction of a phantom (top row) using the operators (35) with $\mu = 1 \cdot 10^{-3}$ and the cutoff function κ_ε defined in (39). The tomographic data was generated in Matlab for the angular range $[-\Phi, \Phi]$, $\Phi = 45°$. The effect of artifact reduction can be clearly observed for $\varepsilon = 20°$ and $\varepsilon = 40°$. However, for $\varepsilon = 20°$, streaks are still visible near $\mathrm{supp}(f)$, whereas for $\varepsilon = 40°$ some visible singularities are smoothed with directions near $\pm 45°$.

smoothing of visible singularities and the visibility of streaks. Due to that fact, the parameter ε has to be chosen carefully in practical reconstructions. Moreover, we would like to note that the use of different cutoff functions κ_ε for the operator $\mathcal{K}_\varepsilon$ may affect the artifact reduction performance. Therefore, a more detailed investigation of practical implementations of our artifact reduction strategy is needed, which is out of

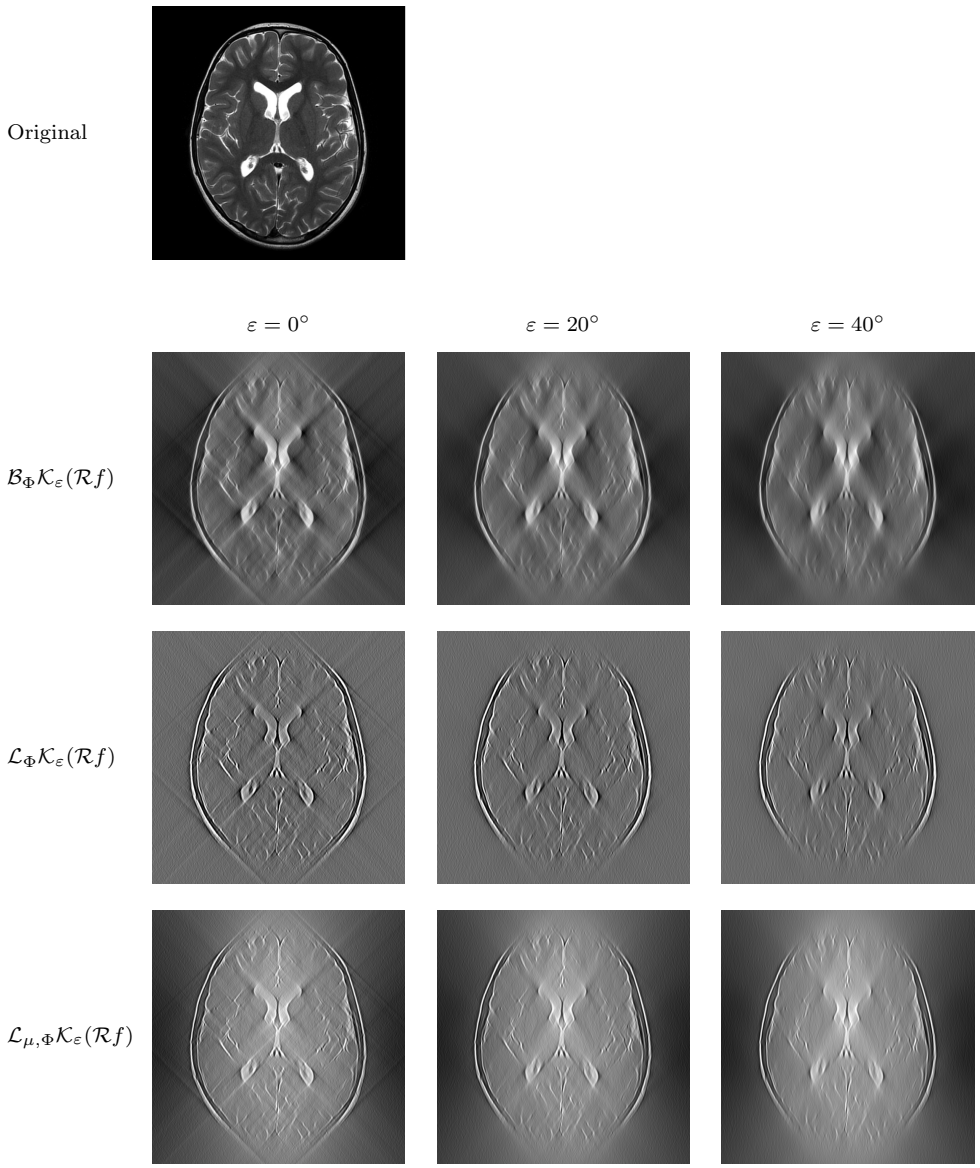

Figure 5 – Reconstruction from noisy Radon data (noise level=1%) of the brain [36] (top row) using the operators (35) with $\mu = 5 \cdot 10^{-4}$ and the cutoff function κ_ε defined in (39). The noisy tomographic data was generated in Matlab for the angular range $[-\Phi, \Phi]$, $\Phi = 45^\circ$. The effect of artifact reduction can be clearly observed for $\varepsilon = 20^\circ$ and $\varepsilon = 40^\circ$. However, some visible singularities are smoothed with directions near $\pm 45^\circ$.

scope of this article.

Furthermore, in our experiments we observed that the noise sensitivity of our modified reconstruction operators (35) is comparable to the sensitivity of standard reconstruction operators (20)-(22), cf. Figures 4 and 5.

6. Concluding Remarks

In this paper we explained why streak artifacts are present in limited angle FBP and Lambda reconstructions and we showed where they occur. We developed a method to reduce those artifacts. To these ends, we provided a thorough mathematical analysis of the reconstruction operators and their microlocal properties. In particular, we explained how to mitigate the streaks. We proved that our modified FBP and Lambda operators are standard pseudodifferential operators, and so they do not add artifacts. In numerical experiments we illustrated that our mathematical results translate into practice. To this end, we used a very fine angular sampling ($\Delta\theta = 0.1^\circ$) in all of our experiments.

We also note that our artifact reduction strategy not only applies to FBP but to all reconstruction algorithms which are based on forward and backprojection operators. For example, an artifact reduced version of the Ladweber iteration $f_n = f_{n-1} + \omega\mathcal{R}_\Phi^*(g - \mathcal{R}_\Phi f_{n-1})$, $0 < \omega \leq \|\mathcal{R}_\Phi\|^{-2}$, can be achieved by replacing the backprojection operator $\mathcal{R}_\Phi^*$ by the weighted backprojection $\mathcal{R}_\Phi^*\mathcal{K}$ at each iteration. Then, an artifact reduced version of the Landweber iteration is given by $f_n = f_{n-1} + \omega\mathcal{R}_\Phi^*\mathcal{K}(g - \mathcal{R}_\Phi f_{n-1})$. This scheme can also be applied to more elaborate reconstruction methods. In [11], for example, the author successfully applied this artifact reduction strategy to the method of curvelet sparse regularization [12] and observed a similar artifact reduction performance as in Figures 4 and 5.

Moreover, we believe that similar weighting should work for fan beam data, and it should help for cone beam data as well and for other limited data problems. The microlocal details would be different, and this is worth exploring.

Finally, we should note that the implementation of our artifact reduction strategy is not yet analyzed for problems with sparse angular sampling which occur in tomosynthesis [29, 40] and in dental CT [19]. Without further analysis, we cannot say how our artifact suppression would work with such data. However, our reduction strategy works well in experiments with noisy non-sparse data. Also, one could analyze how to choose optimal cutoff functions κ_ε. According to the above discussion, a more detailed investigation of practical implementations of our artifact reduction strategy is needed, but this is beyond the scope of this article.

Acknowledgements

The first author was partially supported by the DFG grant No. FI883/3/3-1. He thanks Tufts University for its hospitality during his visits, which facilitated the start of this work. The second author was supported by NSF grants DMS0908015 and DMS1311558 as well as the generosity of the Technische Universität München and the Helmholtz Zentrum, München. He thanks Jan Boman for enlightening discussions about related mathematics, including Lemma A.4, and he thanks Alfred Louis for many stimulating discussions about limited data tomography. Both authors thank Frank Filbir for encouraging and supporting this collaboration. Finally, the authors are indebted to the referees for their thoughtful comments that improved the article and point to future research.

Appendix A. Proof of a Key Theorem and Main Theorems

In this section we prove a theorem that gives the relation between the Fourier transform and each of the operators we consider, and then we use that theorem to prove the results in the article.

We first introduce notation we will use throughout the appendix. The action of a distribution f on a test function ψ will be denoted by $\langle f, \psi \rangle$, and when needed we will indicate the ambient space by $\langle\ ,\ \rangle_{\mathbb{R}^n}$ or $\langle\ ,\ \rangle_{S^1\times\mathbb{R}}$ or $\langle\ ,\ \rangle_{\mathbb{R}}$. The transforms $\mathcal{R}$ and $\mathcal{R}^*$ are defined on distributions by duality. Since $\mathcal{R}^* : \mathcal{E}(S^1 \times \mathbb{R}) \to \mathcal{E}(\mathbb{R}^2)$ is continuous, $\mathcal{R} : \mathcal{E}'(\mathbb{R}^2) \to \mathcal{E}'(S^1 \times \mathbb{R})$ is weakly continuous using the following definition: for $f \in \mathcal{E}'(\mathbb{R}^2)$, $\mathcal{R}f$ is the distribution defined by $\langle \mathcal{R}f, g\rangle_{S^1\times\mathbb{R}} = \langle f, \mathcal{R}^* g\rangle_{\mathbb{R}^2}$, One defines $\mathcal{R}^* : \mathcal{S}'(S^1 \times \mathbb{R}) \to \mathcal{S}'(\mathbb{R}^2)$ in a similar way, and $\mathcal{R}^*$ is weakly continuous, too.

It is clearer and easier to investigate general backprojection operators, not just $\mathcal{R}^*_\Phi$. To this end, we let $\kappa : S^1 \to \mathbb{R}$ be a piecewise smooth bounded function supported in $\mathrm{cl}(S^1_\Phi)$ and, as noted previously, $\mathcal{K}$ is the operator:

$$\mathcal{K} : \mathcal{S}(S^1 \times \mathbb{R}) \to \mathcal{S}'(S^1 \times \mathbb{R}),\ \mathcal{K}g(\theta, s) = \kappa(\theta)g(\theta, s). \tag{A.1}$$

In the process of proving our theorem, we will show $\mathcal{K}$ is defined and weakly continuous on the range of the Radon transform, $\mathcal{R}(\mathcal{E}'(\mathbb{R}^2))$ and on Λ_s of this range.

Theorem A.1 (Key Theorem)**.** *Let $\kappa : S^1 \to \mathbb{R}$ be piecewise continuous and supported in $\mathrm{cl}(S^1_\Phi)$, and let $\mathcal{K}$ be the operator given in* (A.1)*. Let $f \in \mathcal{S}(\mathbb{R}^2)$ and let $\mu \in \mathbb{R}$. Then,*

$$\mathcal{B}_\Phi\mathcal{K}\mathcal{R}f = \frac{1}{4\pi}\mathcal{R}^*\mathcal{K}\Lambda_s\mathcal{R}f \tag{A.2a}$$

$$= \mathcal{F}^{-1}\left(\kappa\left(\frac{\xi}{\|\xi\|}\right)\mathcal{F}f\right) \tag{A.2b}$$

$$= \mathcal{F}^{-1}\left(\kappa\left(\frac{\xi}{\|\xi\|}\right)\right) * f \tag{A.2c}$$

$$\mathcal{L}_{\mu,\Phi}\mathcal{K}\mathcal{R}f = \frac{1}{4\pi}\mathcal{R}^*\mathcal{K}\left(-\frac{d^2}{ds^2} + \mu\right)\mathcal{R}f \tag{A.3a}$$

$$= \mathcal{F}^{-1}\left(\kappa\left(\frac{\xi}{\|\xi\|}\right)\left(\|\xi\| + \frac{\mu}{\|\xi\|}\right)\mathcal{F}f\right) \tag{A.3b}$$

$$= \mathcal{F}^{-1}\left(\kappa\left(\frac{\xi}{\|\xi\|}\right)\left(\|\xi\| + \frac{\mu}{\|\xi\|}\right)\right) * f\,. \tag{A.3c}$$

Each operator making up the transforms in (A.2) *and* (A.3) *is defined, and the transforms are weakly continuous from $\mathcal{E}'(\mathbb{R}^2)$ to $\mathcal{S}'(\mathbb{R}^2)$.*

This theorem will allow us to show the operators in the article are standard pseudodifferential operators when κ is smooth, and it will allow us to analyze the added singularities for the other operators.

Proof. Note that $\mathcal{K}$ commutes with Λ_s and $\left(-\frac{d^2}{ds^2} + \mu\right)$ because they operate on different variables, and, as we will prove, they are defined and weakly continuous on the distributions to which we apply them. This justifies switching $\mathcal{K}$ and these operators in (A.2a) and (A.3a).

First, we prove the formulas for $f \in \mathcal{S}(\mathbb{R}^2)$, and in the process, we show each operation is defined. For $f \in \mathcal{S}(\mathbb{R}^2)$, $\mathcal{R}f \in \mathcal{S}(S^1 \times \mathbb{R})$ [15], and so $\Lambda_s \mathcal{R} f$ is a smooth function (because its Fourier transform in s is rapidly decreasing at infinity and smooth in θ). Then, $\mathcal{K}\Lambda_s\mathcal{R}f$ is a piecewise continuous function and, therefore, $\mathcal{R}^*\mathcal{K}\Lambda_s\mathcal{R}f$ is defined. This allows us to do the following calculation using the Fourier slice theorem (cf. [27]), $\mathcal{F}_s(\mathcal{R}f)(\theta,\tau) = \sqrt{2\pi}\widehat{f}(\tau\theta)$:

$$\begin{aligned}
\mathcal{R}^*\mathcal{K}\Lambda_s\mathcal{R}f(x) &= \int_{S^1} \kappa(\theta)\Lambda_s\mathcal{R}f(\theta, x\cdot\theta)\,\mathrm{d}\theta && \text{(A.4)}\\
&= \frac{1}{\sqrt{2\pi}}\int_{S^1}\kappa(\theta)\int_{-\infty}^{\infty} e^{i\tau x\cdot\theta}\,|\tau|\,\mathcal{F}_s\mathcal{R}f(\theta,\tau)\,\mathrm{d}\tau\,\mathrm{d}\theta\\
&= 2\int_{S^1}\int_0^{\infty} e^{ix\cdot\tau\theta}\,\kappa\left(\frac{\tau\theta}{\tau}\right)\widehat{f}(\tau\theta)\tau\,\mathrm{d}\tau\,\mathrm{d}\theta\\
&= 2\int_{\xi\in\mathbb{R}^2} e^{ix\cdot\xi}\,\kappa\left(\frac{\xi}{\|\xi\|}\right)\widehat{f}(\xi)\,\mathrm{d}\xi\,. && \text{(A.5)}\\
&= 4\pi\mathcal{F}^{-1}\left(\kappa\left(\frac{\xi}{\|\xi\|}\right)\mathcal{F}f\right) && \text{(A.6)}
\end{aligned}$$

and now the equality between parts (A.2a)-(A.2c) is easy to show. One can see from (A.6) that the Fourier transform of $\mathcal{R}^*\mathcal{K}\Lambda_s\mathcal{R}f$ is rapidly decreasing at infinity, so $\mathcal{R}^*\mathcal{K}\Lambda_s\mathcal{R}f \in \mathcal{E}(\mathbb{R}^2)$ if $f \in \mathcal{S}(\mathbb{R}^2)$.

The proof of (A.3) for $f \in \mathcal{S}(\mathbb{R}^2)$ is similar.

We now prove that formulas (A.2a)-(A.2b) are valid in a distributional sense for $f \in \mathcal{E}'(\mathbb{R}^2)$. Part (A.2c) is just a different way of writing (A.2b) using properties of the Fourier transform and convolution (which are valid for distributions in $\mathcal{S}'$, if one of them has compact support [17, Theorem 7.1.15]).

First, we show the left-hand side of (A.2a) is defined and then we show it is weakly continuous for $f \in \mathcal{E}'(\mathbb{R}^2)$. Then, we prove that the expression in (A.2b) is weakly continuous. Since we have shown these right sides of (A.2) are equal for $f \in \mathcal{D}(\mathbb{R}^2)$, this will show that they are equal for $f \in \mathcal{E}'(\mathbb{R}^2)$.

For $f \in \mathcal{E}'(\mathbb{R}^2)$, we claim $\mathcal{R}^*\mathcal{K}\Lambda_s\mathcal{R}f$ is a distribution in $\mathcal{S}'(\mathbb{R}^2)$ and each of the operators in the composition is defined. Since $\mathcal{R} : \mathcal{E}'(\mathbb{R}^2) \to \mathcal{E}'(S^1\times\mathbb{R})$ is continuous and $\Lambda_s : \mathcal{E}'(S^1\times\mathbb{R}) \to \mathcal{S}'(S^1\times\mathbb{R})$ is continuous, we have that $\Lambda_s\mathcal{R} : \mathcal{E}'(\mathbb{R}^2) \to \mathcal{S}'(S^1\times\mathbb{R})$ is continuous. Proposition 1.09 and Remark 1.10 in [16] show that for $f \in \mathcal{E}'(\mathbb{R}^2)$, $\mathcal{R}f \in C^\infty(S^1, \mathcal{E}'(\mathbb{R}))$. This means that for each $\theta \in S^1$, $\mathcal{R}f(\theta,\cdot)$ is a distribution in $\mathcal{E}'(\mathbb{R})$ and $\theta \mapsto \mathcal{R}f(\theta,\cdot)$ is a smooth function from S^1 to $\mathcal{E}'(\mathbb{R})$. Since Λ_s can be viewed as an operator from : $\mathcal{E}'(\mathbb{R})$ to $\mathcal{S}'(\mathbb{R})$, the function $\theta \mapsto \kappa(\theta)\Lambda_s\mathcal{R}f(\theta,\cdot)$ is a piecewise continuous map from S^1 to $\mathcal{S}'(\mathbb{R})$. Therefore, for $g \in \mathcal{S}(S^1\times\mathbb{R})$, the integral

$$\int_{\theta\in S^1}\kappa(\theta)\,\langle\Lambda_s\mathcal{R}f(\theta,\cdot), g(\theta,\cdot)\rangle_{\mathbb{R}}\;\mathrm{d}\theta \qquad \text{(A.7)}$$

is defined. Since this integral is equal to $\langle\mathcal{K}\Lambda_s\mathcal{R}f, g\rangle$ for $f \in \mathcal{S}(\mathbb{R}^2)$, this allows us to define $\mathcal{K}\Lambda_s\mathcal{R}$ on distributions using this integral (A.7):

$$\begin{aligned}
\langle\mathcal{K}\Lambda_s\mathcal{R}f, g\rangle &= \int_{\theta\in S^1}\kappa(\theta)\,\langle\Lambda_s\mathcal{R}f(\theta,\cdot), g(\theta,\cdot)\rangle_{\mathbb{R}}\;\mathrm{d}\theta && \text{(A.8)}\\
&= \sqrt{2\pi}\int_{\theta\in S^1}\kappa(\theta)\int_{\tau\in\mathbb{R}}|\tau|\,\mathcal{F}f(\tau\theta)\mathcal{F}_s^{-1}g(\theta,\tau)\,\mathrm{d}\tau\,\mathrm{d}\theta\,. && \text{(A.9)}
\end{aligned}$$

The integral in (A.8) is equal to the integral (A.9) by duality of the Fourier transform and the Fourier Slice theorem, which is true for $\mathcal{E}'$ by, e.g., [16, Proposition 1.13]. Since $g \in \mathcal{S}(S^1 \times \mathbb{R})$, and $f \in \mathcal{E}'(\mathbb{R}^2)$ (so $\mathcal{F}f$ is a polynomially increasing function), this integral converges. One uses the integral (A.9) to show $\mathcal{K}\Lambda_s\mathcal{R}f$ is a distribution in $\mathcal{S}'(S^1 \times \mathbb{R})$ (i.e., a continuous linear functional on $\mathcal{S}$): if $g_j \to g$ in $\mathcal{S}(S^1 \times \mathbb{R})$ then, since $\mathcal{F}_s^{-1}$ is continuous on $\mathcal{S}$, $\mathcal{F}_s^{-1}g_j \to \mathcal{F}_s^{-1}g$ in $\mathcal{S}$ and therefore

$$\sqrt{2\pi}\int_{\theta\in S^1}\kappa(\theta)\int_{\tau\in\mathbb{R}}|\tau|\mathcal{F}f(\tau\theta)\mathcal{F}_s^{-1}g_j(\theta,\tau)\,\mathrm{d}\tau\,\mathrm{d}\theta$$
$$\longrightarrow\ \sqrt{2\pi}\int_{\theta\in S^1}\kappa(\theta)\int_{\tau\in\mathbb{R}}|\tau|\,\mathcal{F}f(\tau\theta)\mathcal{F}_s^{-1}g(\theta,\tau)\,\mathrm{d}\tau\,\mathrm{d}\theta$$

as $j \to \infty$ by dominated convergence. Finally, since $\mathcal{R}^* : \mathcal{S}'(S^1 \times \mathbb{R}) \to \mathcal{S}'(\mathbb{R}^2)$ is continuous, $\mathcal{R}^*\mathcal{K}\Lambda_s\mathcal{R}f$ is defined as a tempered distribution for $f \in \mathcal{E}'(\mathbb{R}^2)$.

We now prove that the functional

$$\mathcal{E}'(\mathbb{R}^2) \ni f \mapsto \mathcal{K}\Lambda_s\mathcal{R}f$$

is weakly continuous to $\mathcal{S}'(S^1 \times \mathbb{R})$. Let $f_j \to f$ weakly in $\mathcal{E}'(\mathbb{R}^2)$ and let $g \in \mathcal{S}(S^1 \times \mathbb{R})$. Using (A.8), we get

$$\langle\mathcal{K}\Lambda_s\mathcal{R}f_j, g\rangle_{S^1\times\mathbb{R}} = \int_{\theta\in S^1}\kappa(\theta)\left\langle\mathcal{R}f_j(\theta,\cdot), \Lambda_s^t g(\theta,\cdot)\right\rangle_{\mathbb{R}}\,\mathrm{d}\theta \tag{A.10}$$
$$= \int_{\theta\in S^1}\kappa(\theta)\left\langle f_j(x), \Lambda_s^t g(\theta, x\cdot\theta)\right\rangle_{\mathbb{R}^2}\,\mathrm{d}\theta \tag{A.11}$$

where $\Lambda_s^t = \mathcal{F}_s\,|\tau|\,\mathcal{F}_s^{-1}$. To get from (A.10) to (A.11), note that the dual of $\mathcal{R}_\theta f := \mathcal{R}f(\theta,\cdot)$ (for fixed θ) is $\mathcal{R}_\theta^* g = g(\theta, x\cdot\theta)$.

To finish the proof that $\mathcal{R}^*\mathcal{K}\Lambda_s\mathcal{R}f$ is weakly continuous, we show we can switch the evaluation $\langle\ ,\ \rangle_{\mathbb{R}^2}$ and the integral in (A.11). For each fixed j, f_j is a distribution in $\mathcal{E}'(\mathbb{R}^2)$ so it has finite order and fixed compact support. Since $g \in \mathcal{S}(S^1 \times \mathbb{R})$, the map $\theta \mapsto \Lambda_s g(\theta, x\cdot\theta)$ is a smooth function of $\theta \in S^1$ that is bounded along with all of its derivatives for $\theta \in S^1$ and for $x \in \mathrm{supp}(f_j)$. Since S^1 is compact and κ is piecewise continuous in θ, we can use limits of Riemann sums to justify switching the evaluation with f_j and the integral in θ to get

$$\langle\mathcal{K}\Lambda_s\mathcal{R}f_j, g\rangle_{S^1\times\mathbb{R}} = \left\langle f_j(x), \int_{\theta\in S^1}\kappa(\theta)\Lambda_s g(\theta, x\cdot\theta)\,\mathrm{d}\theta\right\rangle_{\mathbb{R}^2}. \tag{A.12}$$

Now, because S^1 is compact, and $\Lambda_s g$ is smooth, the function

$$x \mapsto \int_{\theta\in S^1}\kappa(\theta)\Lambda_s g(\theta, x\cdot\theta)\,\mathrm{d}\theta$$

is C^∞. Since $f_j \to f$ weakly in $\mathcal{E}'(\mathbb{R}^2)$, the expression in (A.12) goes to

$$\langle\mathcal{K}\Lambda_s\mathcal{R}f, g\rangle_{S^1\times\mathbb{R}} = \left\langle f(x), \int_{\theta\in S^1}\kappa(\theta)\Lambda_s g(\theta, x\cdot\theta)\,\mathrm{d}\theta\right\rangle_{\mathbb{R}^2},$$

and so $\mathcal{K}\Lambda_s\mathcal{R}$ is continuous from $\mathcal{E}'(\mathbb{R}^2)$ to $\mathcal{S}'(S^1 \times \mathbb{R})$. Since $\mathcal{R}^*$ is weakly continuous from $\mathcal{S}'(S^1 \times \mathbb{R})$ to $\mathcal{S}'(\mathbb{R}^2)$, we see that $\mathcal{R}^*\mathcal{K}\Lambda_s\mathcal{R}$ is weakly continuous from $\mathcal{E}'(\mathbb{R}^2)$ to $\mathcal{S}'(\mathbb{R}^2)$.

Finally, we will prove that the expression in (A.2b) is weakly continuous for $f \in \mathcal{E}'(\mathbb{R}^2)$. As discussed above, this will show (A.2) holds for $f \in \mathcal{E}'(\mathbb{R}^2)$.

Let $h \in \mathcal{S}(\mathbb{R}^2)$ and let $f_j \to f$ weakly in $\mathcal{E}'(\mathbb{R}^2)$. Then,

$$\left\langle \mathcal{F}^{-1}\kappa\left(\frac{\xi}{\|\xi\|}\right)\mathcal{F}f_j, h\right\rangle = \left\langle f_j, \mathcal{F}^{-1}\left[\kappa\left(\frac{\xi}{\|\xi\|}\right)\mathcal{F}h\right]\right\rangle \tag{A.13}$$

and $\mathcal{F}^{-1}\left[\kappa\left(\frac{\xi}{\|\xi\|}\right)\mathcal{F}h\right]$ is C^∞ since the expression in square brackets is rapidly decreasing as $\mathcal{F}h \in \mathcal{S}(\mathbb{R}^2)$ and κ is bounded. Using equation (A.13) we see

$$\begin{aligned}\left\langle \mathcal{F}^{-1}\kappa\left(\frac{\xi}{\|\xi\|}\right)\mathcal{F}f_j, h\right\rangle &= \left\langle f_j, \mathcal{F}^{-1}\left[\kappa\left(\frac{\xi}{\|\xi\|}\right)\mathcal{F}h\right]\right\rangle \\ \to \left\langle f, \mathcal{F}^{-1}\left[\kappa\left(\frac{\xi}{\|\xi\|}\right)\mathcal{F}h\right]\right\rangle &= \left\langle \mathcal{F}^{-1}\kappa\left(\frac{\xi}{\|\xi\|}\right)\mathcal{F}f, h\right\rangle\end{aligned}$$

Thus (A.2) holds for $f \in \mathcal{E}'(\mathbb{R}^2)$, and this finishes the proof for $\mathcal{B}_\Phi$.

The proof for (A.3) is similar but easier since one can use the fact that

$$\left(-\frac{d^2}{ds^2} + \mu\right)\mathcal{R}f = \mathcal{R}\left(\left(-\Delta + \mu\right)f\right)$$

and prove the theorem for $\mathcal{R}^*\mathcal{K}\mathcal{R}$. □

Proof of Theorem 2.1. This theorem follows from Theorem A.1 by writing $\mathcal{R}_\Phi^* = \mathcal{R}^*\mathcal{K}_\Phi$ where $\mathcal{K}_\Phi$ is the operator that multiplies by $\kappa(\theta) = \chi_{S_\Phi^1}$ (see Remark 1). For $\mathcal{B}_\Phi$, we apply equality (A.2a) and (A.2b) with this κ. For $\mathcal{L}_{\mu,\Phi}$, we use a similar argument using A.1, equations (A.3a) and (A.3b). These formulas are valid for $f \in \mathcal{E}'(\mathbb{R}^2)$ as well as for $f \in \mathcal{S}(\mathbb{R}^2)$. □

Proof of Theorem 4.1. First, we show $\mathrm{WF}_\Phi(f) \subset \mathrm{WF}(\mathcal{H}(\mathcal{R}f))$. This part uses Theorem 4.2 (which is proved independently of this theorem) and the following useful lemma.

Lemma A.2. *Let u be a distribution in $\mathcal{S}'(\mathbb{R}^n)$ such that $\hat{u}$ is a locally integrable function bounded at infinity by a polynomial in $\|\xi\|$. Assume that $\hat{u}$ is supported away from the open cone V. Then for any $x \in \mathbb{R}^n$, and any $\xi \in V$, $(x,\xi) \notin \mathrm{WF}(u)$.*

Note that if $u \in \mathcal{E}'(\mathbb{R}^n)$ then this follows immediately from the definition of wavefront set and (25). The proof for our case is identical to the proof of Lemma 8.1.1 in [17] because of our growth assumptions for $\hat{u}$.

Getting back to the theorem, we prove the left-hand containment of (32) for $\mathcal{B}_\Phi$. We let $\xi_0 \in W_\Phi$ and let φ be a smooth cutoff function supported in S_Φ^1 and equal to 1 in a neighborhood of $\frac{\xi_0}{\|\xi_0\|}$. Let $\mathcal{K}_\varphi$ be the multiplier operator in (34) with $\kappa = \varphi$. Then, by Theorem 4.2, $\mathcal{B}_\Phi\mathcal{K}_\varphi\mathcal{R}$ is a standard pseudodifferential operator of order zero with symbol $\varphi\left(\frac{\xi}{\|\xi\|}\right)$, which is elliptic near ξ_0. So, if $(x_0,\xi_0) \in \mathrm{WF}(f)$, then $(x_0,\xi_0) \in \mathrm{WF}(\mathcal{B}_\Phi\mathcal{K}_\varphi\mathcal{R}f)$. Now, note that

$$\mathcal{F}\left(\mathcal{B}_\Phi\left(1 - \mathcal{K}_\varphi\right)\mathcal{R}f\right) = \left(\chi_{W_\Phi} - \varphi\left(\frac{\xi}{\|\xi\|}\right)\right)\mathcal{F}f,$$

and since this Fourier transform is zero on a conic neighborhood of ξ_0, $\mathcal{B}_\Phi\left(1-\mathcal{K}_\varphi\right)\mathcal{R}f$ is smooth in direction ξ_0 at all points by Lemma A.2. Therefore, since $(x_0,\xi_0)\in \mathrm{WF}(\mathcal{B}_\Phi\mathcal{K}_\varphi\mathcal{R}f)$, $(x_0,\xi_0)\in\mathrm{WF}(\mathcal{B}_\Phi\mathcal{R}f)$. This proves the left containment of (32) for $\mathcal{B}_\Phi$. The proofs for $\mathcal{L}_\Phi$ and $\mathcal{L}_{\mu,\Phi}$ are similar.

We now prove the right hand containment in (32) in Theorem 4.1 for $\mathcal{B}_\Phi$.

We let $u_\Phi(x)=\chi_{W_\Phi}(x)$ and $\check{u}_\Phi=\mathcal{F}^{-1}(u_\Phi)$. Then $u_\Phi,\check{u}_\Phi\in\mathcal{S}'(\mathbb{R}^2)$ and

$$\mathcal{B}_\Phi\mathcal{R}f=P_\Phi f=\frac{1}{4\pi}f*\check{u}_\Phi,$$

which is true by Theorem A.1 equation (A.2c) for $\kappa=u_\Phi$. An important result in microlocal analysis gives us the wavefront set of convolutions.

Lemma A.3 ([17, Equation (8.2.16), p. 270])**.** *Let f and g be distributions such that either f or g has compact support. Then,*

$$\mathrm{WF}(f*g)\subseteq\left\{(x+y,\xi)\in\mathbb{R}^2\times\mathbb{R}^2_*:(x,\xi)\in\mathrm{WF}(f),\,(y,\xi)\in\mathrm{WF}(g)\right\}.$$

Then by Lemma A.3 we have

$$\mathrm{WF}(\mathcal{B}_\Phi\mathcal{R}f)\subseteq\left\{(x+y,\xi)\in\mathbb{R}^2\times\mathbb{R}^2_*:(x,\xi)\in\mathrm{WF}(f),\,(y,\xi)\in\mathrm{WF}(\check{u}_\Phi)\right\}. \quad (A.14)$$

Now observe that $\check{u}_\Phi$ is homogeneous since u_Φ is homogeneous, and our next lemma gives the wavefront of a homogeneous distribution.

Lemma A.4 ([17, Theorem 8.1.8])**.** *Let $u\in\mathcal{S}'(\mathbb{R}^2)$ be homogeneous in $\mathbb{R}^2_*$, then*

$$(x,\xi)\in\mathrm{WF}(u)\;\Leftrightarrow\;(\xi,-x)\in\mathrm{WF}(\widehat{u}\,),\quad \textit{whenever } \xi\neq0 \textit{ and } x\neq0 \quad (A.15)$$

$$(0,\xi)\in\mathrm{WF}(u)\Leftrightarrow\xi\in\mathrm{supp}(\hat{u}). \quad (A.16)$$

Therefore, by Lemma A.4 it suffices to compute the wavefront set $\mathrm{WF}(u_\Phi)$. To this end, we first note that

$$\mathrm{sing\,supp}\,(u_\Phi)=\partial W_\Phi=(\mathbb{R}\cdot\theta(\Phi))\cup(\mathbb{R}\cdot\theta(-\Phi)), \quad (A.17)$$

and so the wavefront set of u_Φ for points $x\neq0$ is the set of normals to W_Φ, so outside of the origin points in the wavefront set of u_Φ can be written

$$\left(\alpha\theta(\phi),r\theta^\perp(\phi)\right)\quad\text{where }\alpha\in\mathbb{R}_*,\ r\in\mathbb{R}_*\text{ and }\phi=\pm\Phi \quad (A.18)$$

By (A.16), we see that the localized frequency set for $x=0$ is

$$\Sigma_0(\check{u}_\Phi)=\overline{W}_\Phi. \quad (A.19)$$

Now, using Lemma A.4 and equation (A.18) and finally equation (A.19), we have

$$\mathrm{WF}(\check{u}_\Phi)=\left\{(r\theta^\perp(\phi),\alpha\theta(\phi)):r,\alpha\in\mathbb{R}_*,\,\phi=\pm\Phi\right\}\cup\left(\{0\}\times\overline{W}_\Phi\right). \quad (A.20)$$

Equation (32) in the theorem follows now by inserting (A.20) into (A.14) and using the definition of $\mathcal{A}_\Phi(f)$, (33).

To prove the theorem for $\mathcal{L}_\Phi$ we use a similar proof but starting with Theorem A.1 and equation (A.3). We replace u_Φ by $u_\Phi(\xi)\,\|\xi\|$ and repeat the proof above since $u_\Phi(\xi)\,\|\xi\|$ is a homogeneous distribution with singular support ∂W_Φ. For $\mathcal{L}_{\mu,\Phi}$ we use a similar proof to show (A.20) for the homogeneous distribution $u_\Phi(\xi)\frac{\mu}{\|\xi\|}$ and then use the fact that the wavefront set of a sum is contained in the union of the wavefront sets.

□

Proof of Theorem 4.2. Theorem A.1 and expressions (A.2b)-(A.3b) show that these operators have the form of pseudodifferential operators. Since κ is smooth on $\mathbb{R}^2_*$ and is homogeneous of degree zero, each of the symbols of the operators in (A.2b)-(A.3b) is a standard smooth symbol, so each operator is a standard pseudodifferential operator. Here we are using the fact that operators as in (31) that include sums of homogeneous symbols differ by smoothing operators from pseudodifferential operators with C^∞ symbols. This is discussed after (31). Since (A.2)-(A.3) are exact formulas, these symbols are full symbols, not just top-order symbols. □

Proof of Corollary 4.3. Since the support of the symbols given in (36) contains $W_{\Phi'}$, each of the operators is a standard pseudodifferential operator that is elliptic in $\mathbb{R}^2 \times W_{\Phi'}$, and this explains the left containment in (37). By Lemma A.2, $\mathcal{HR}f$ is smooth in directions outside of $\overline{W}_\Phi$ and this justifies right-hand containment in (37).

Now, consider the operator $\mathcal{M} = (\mathcal{B}_\Phi \mathcal{KR} - \mathcal{B}_\Phi \mathcal{R})$. It's Fourier transform can be written

$$\mathcal{F}(\mathcal{M}f) = \left[\chi_\Phi\left(\frac{\xi}{\|\xi\|}\right) - \kappa\left(\frac{\xi}{\|\xi\|}\right)\right]\mathcal{F}f(\xi),$$

and this Fourier transform is zero for $\xi \in W_{\Phi'}$ since $\kappa\left(\frac{\xi}{\|\xi\|}\right) = 1$ on that set. Then, by Lemma A.2, $\mathcal{M}f$ is smooth in directions on $W_{\Phi'}$ and so $\mathcal{M}$ is a smoothing operator in those directions. The proofs for the other operators are almost the same. □

References

[1] G. Ambartsoumian, R. Felea, V. Krishnan, C. Nolan, and E. T. Quinto. A class of singular Fourier integral operators in synthetic aperture radar imaging. *Journal of Functional Analysis*, 264:246–269, 2013.

[2] M. Davison and F. Grünbaum. Tomographic Reconstruction with Arbitrary Directions. *Comm. Pure Appl. Math.*, 34:77–120, 1981.

[3] D. J. De Rosier and A. Klug. Reconstruction of Three Dimensional Structures from Electron Micrographs. *Nature*, 217(5124):130–134, Jan. 1968.

[4] J. T. Dobbins III. Tomosynthesis imaging: At a translational crossroads. *Medical Physics*, 36(6):1956–1967, 2009.

[5] J. T. Dobbins III and D. J. Godfrey. Digital x-ray tomosynthesis: current state of the art and clinical potential. *Physics in Medicine and Biology*, 48(19):R65 – R106, 2003.

[6] A. Faridani, D. Finch, E. L. Ritman, and K. T. Smith. Local tomography, II. *SIAM J. Appl. Math.*, 57:1095–1127, 1997.

[7] A. Faridani, E. L. Ritman, and K. T. Smith. Local tomography. *SIAM J. Appl. Math.*, 52:459–484, 1992.

[8] R. Felea and E. T. Quinto. The microlocal properties of the local 3-D spect operator. *SIAM J. Math. Anal.*, 43(3):1145–1157, 2011.

[9] D. V. Finch, I.-R. Lan, and G. Uhlmann. Microlocal Analysis of the Restricted X-ray Transform with Sources on a Curve. In G. Uhlmann, editor, *Inside Out, Inverse Problems and Applications*, volume 47 of *MSRI Publications*, pages 193–218. Cambridge University Press, 2003.

[10] F. G. Friedlander. *Introduction to the theory of distributions*. Cambridge University Press, Cambridge, second edition, 1998. With additional material by M. Joshi.

[11] J. Frikel. *Reconstructions in limited angle x-ray tomography: Characterization of classical reconstructions and adapted curvelet sparse regularization*. PhD thesis, Technische Universität München, 2013. URL: `https://mediatum.ub.tum.de/node?id=1115037`.

[12] J. Frikel. Sparse regularization in limited angle tomography. *Applied and Computational Harmonic Analysis*, 34(1):117–141, Jan. 2013.

[13] A. Greenleaf and G. Uhlmann. Non-local inversion formulas for the X-ray transform. *Duke Math. J.*, 58:205–240, 1989.

[14] F. A. Grünbaum. A study of fourier space methods for "limited angle" image reconstruction. *Numerical Functional Analysis and Optimization*, 2(1):31–42, Jan. 1980.
[15] S. Helgason. The Radon transform on Euclidean spaces, compact two-point homogeneous spaces and Grassman manifolds. *Acta Math.*, 113:153–180, 1965.
[16] A. Hertle. Continuity of the Radon transform and its inverse on Euclidean space. *Mathematische Zeitschrift*, 184:165–192, 1983.
[17] L. Hörmander. *The analysis of linear partial differential operators. I.* Classics in Mathematics. Springer-Verlag, Berlin, 2003. Distribution theory and Fourier analysis, Reprint of the second (1990) edition [Springer, Berlin].
[18] N. Hyvönen, M. Kalke, M. Lassas, H. Setälä, and S. Siltanen. Three-dimensional dental X-ray imaging by combination of panoramic and projection data. *Inverse Problems and Imaging*, 4(2):257–271, May 2010.
[19] N. Hyvönen, M. Kalke, M. Lassas, H. Setälä, and S. Siltanen. Three-dimensional Dental X-ray Imaging by Combination of Panoramic and Projection Data. *Inverse Problems and Imaging*, 4:257–271, 2010.
[20] T. Inouye. Image Reconstruction with Limited Angle Projection Data. *Proceedings of IEEE Transactions on Nuclear Science*, 26(2):2665–2669, Apr. 1979.
[21] P. Kuchment, K. Lancaster, and L. Mogilevskaya. On local tomography. *Inverse Problems*, 11:571–589, 1995.
[22] A. K. Louis. Picture reconstruction from projections in restricted range. *Math. Methods Appl. Sci.*, 2(2):209–220, 1980.
[23] A. K. Louis. Incomplete data problems in X-ray computerized tomography I. Singular value decomposition of the limited angle transform. *Numerische Mathematik*, 48:251–262, 1986.
[24] A. K. Louis. Combining Image Reconstruction and Image Analysis with an Application to Two-Dimensional Tomography. *SIAM J. Img. Sci.*, 1:188–208, 2008.
[25] J. Ludwig, T. Mertelmeier, H. Kunze, and W. Härer. A novel approach for filtered backprojection in tomosynthesis based on filter kernels determined by iterative reconstruction techniques. In *Digital Mammography / IWDM*, volume 5116 of *Lecture Notes in Computer Science*, pages 612–620. Springer, 2008.
[26] J. L. Mueller and S. Siltanen. *Linear and Nonlinear Inverse Problems with Practical Applications*. SIAM, October 2012.
[27] F. Natterer. *The mathematics of computerized tomography*. B. G. Teubner, Stuttgart, 1986.
[28] F. Natterer and F. Wübbeling. *Mathematical methods in image reconstruction*. SIAM Monographs on Mathematical Modeling and Computation. Society for Industrial and Applied Mathematics (SIAM), Philadelphia, PA, 2001.
[29] L. T. Niklason et al. Digital tomosynthesis in breast imaging. *Radiology*, 205(2):399–406, 1997.
[30] X. Pan, E. Y. Sidky, and M. Vannier. Why do commercial CT scanners still employ traditional, filtered back-projection for image reconstruction? *Inverse Problems*, 25(12):123009, 2009.
[31] A. Peres. Tomographic Reconstruction from Limited Angular Data. *Journal of Computer Assisted Tomography*, 3(6):800–808003, Dec. 1979.
[32] B. Petersen. *Introduction to the Fourier Transform and Pseudo-Differential Operators*. Pittman, Boston, 1983.
[33] E. T. Quinto. Singularities of the X-ray transform and limited data tomography in $\mathbb{R}^2$ and $\mathbb{R}^3$. *SIAM J. Math. Anal.*, 24(5):1215–1225, 1993.
[34] E. T. Quinto and O. Öktem. Local tomography in electron microscopy. *SIAM J. Appl. Math.*, 68:1282–1303, 2008.
[35] E. T. Quinto and H. Rullgård. Local singularity reconstruction from integrals over curves in R^3. *Inverse Problems and Imaging*, 7(2):585–609, 2013.
[36] Radiopedia.org. 2010. `http://radiopaedia.org`.
[37] A. G. Ramm. Inversion of Limited Angle Tomographic data. *Computers & Mathematics with Applications*, 22(4/5):101–111, 1991.
[38] A. G. Ramm. Inversion of limited angle tomographic data II. *Applied Mathematics Letters*, 5(2):47–49, 1992.
[39] A. G. Ramm and A. Katsevich. *The Radon Transform and Local Tomography*. CRC Press, Boca Raton, FL, 1996.
[40] I. Reiser, J. Bian, R. Nishikawa, E. Sidley, and X. Pan. Comparison of reconstruction algorithsm for digital breast tomosynthesis. Technical report, University of Chicago, 2009. arXiv:0908.2610v1, phyusics.med-ph.
[41] K. Sandberg, D. N. Mastronarde, and G. Beylkin. A fast reconstruction algorithm for electron microscope tomography. *Journal of Computational and Applied Mathematics*, 144(1-2):61–72, Oct. 2003.

[42] W. C. Scarfe, A. G. Farman, and P. Sukovic. Clinical Applications of Cone-Beam Computed Tomography in Dental Practice. Feb. 2006. URL: `http://www.orthodent3d.com/news-resources/Clinical%20Applications%20of%20Cone-Beam%20Computed%20Tomography.pdf`.

[43] P. Stefanov and G. Uhlmann. Is a curved flight path in SAR better than a straight one? *SIAM J. Appl. Math.*, 73(4):1596–1612, 2013.

[44] H. Tuy. Reconstruction of a Three-dimensional Object from a Limited Range of Views. *J. Math. Anal. Appl.*, 80:598–616, 1981.

[45] E. Vainberg, I. A. Kazak, and V. P. Kurozaev. Reconstruction of the internal three-dimensional structure of objects based on real-time integral projections. *Soviet Journal of Nondestructive Testing*, 17:415–423, 1981.